Formation of ordered structures of NO on Rh(111)

J. H. A. Hagelaar, A. P. J. Jansen, and C. F. J. Flipse*
Molecular Materials and Nanosystems/Laboratory of Inorganic Chemistry and Catalysis, Eindhoven University of Technology, P.O. Box 513, 5600 MB Eindhoven, The Netherlands
(Received 24 November 2008; published 12 March 2009)

In this work, several (unreported) structures of NO on Rh(111) are presented for coverages ranging from 0–0.78 ML. The formation of these structures as evidenced experimentally by scanning tunneling microscopy (STM) images is explained using density-functional theory derived values for the lateral interactions and adsorption energies of NO on Rh(111). Kinetic Monte Carlo simulations using the derived lateral interactions are performed to determine structures at finite temperatures. The resulting structures can be directly compared to the molecular arrangements observed in the STM experiment. The configuration of the first three structures that form for increasing coverage is the same both experimentally and theoretically. In all three structures, the molecules only occupy the fcc and hcp adsorption sites. Yet, at high coverage, at which the top adsorption sites become occupied, a discrepancy arises.

DOI: 10.1103/PhysRevB.79.115414 PACS number(s): 68.43.Fg, 68.37.Ef, 64.60.De

I. INTRODUCTION

The binding strength of molecules adsorbed on a surface can be perturbed by the presence of neighboring species. These lateral interactions between adsorbates can be direct or indirect in nature.[1–7] Interactions in which the substrate is involved are considered indirect and can be divided into electronic and elastic interactions. Electronic interactions alter the binding strength when a substrate atom is shared by several adsorbates and elastic interactions are binding perturbations due to changes in the substrate's surface geometry induced by other adsorbates. Direct interactions, on the other hand, have an electrostatic or a chemical origin. When the molecules' dipole moments are all oriented in the same direction, the electrostatic dipole-dipole coupling can destabilize the adsorbate-surface bond. Alternating dipoles, however, can stabilize this bond. Finally, chemical interactions arise from the overlap of orbitals of neighboring molecules.

Together, the lateral interactions are responsible for the formation of specific adlayer structures of the adsorbates on the surface and this relationship will be studied in this paper. Notice that not only the configuration of the formed structures can be influenced by the interactions but also reaction rates and hence the selectivity of processes. It might even become feasible to make use of them as they can change reaction routes that would otherwise be unfavorable[8] and in the end, more efficient catalytic processes could be made.

Different techniques can be used to quantify lateral interactions. The experimental results obtained from methods like calorimetry and temperature programmed desorption (TPD) have been simulated by kinetic Monte Carlo (kMC) calculations to obtain the lateral interactions by fitting the simulated curve to the experimental one.[9,10] Field ion microscopy (FIM) and later on scanning tunneling microscopy (STM) were used to derive pairwise lateral interactions from the distribution of molecules over the surface.[11–15]

It is important to note that, at finite temperatures, it is not the adlayer structure with minimal internal energy U that forms, but with minimal free energy:

$$A = U - TS, \tag{1}$$

where T is the temperature and S is the entropy of the system. Suppose structures A and B are the only configurations possible for a certain coverage and that $U_A < U_B$ and $S_A < S_B$. Obviously at zero temperature $A = U$ and structure A will form. However, as the importance of the entropy increases with temperature, there is a certain temperature at which structure B has the lowest free energy and prevails. Although the structure having the lowest free energy will form, it is the structure with minimal U from which the lateral interactions should be determined. Usually, the complication of entropy is overcome by taking the limit of zero coverage.[11,14,16] Theoretically, the lateral interactions can be directly derived from total energy (U) calculations of different coverages using density-functional theory (DFT).[17–19] The effect of entropy is included by performing kinetic Monte Carlo simulations using the obtained lateral interactions.[20] Recently, it was shown using STM that pairwise interactions are not always sufficient to describe the formed patterns[16,17] and many-body effects have to be taken into account.

While studying the system of NO molecules on a Rh(111) substrate by STM at different coverages, we found a large number of (unreported) adlayer structures. This wide variety of ordered structures makes the system a good candidate for the accurate determination of lateral interactions. Similar to[20] three of the above described methods are used to determine the lateral interactions. Experimentally, structures of NO adsorbed at 200 K on a Rh(111) single crystal are studied in real space by STM. On the theoretical side, kMC simulations using DFT derived values for the lateral interactions are performed. As kMC includes entropy effects, the thus calculated structures can be directly compared to the structures observed in the experiment.

From previous studies it is known that NO adsorbs molecularly on Rh(111) at low coverage below $T \sim 250$ K. Two different ordered structures have been reported using low-energy electron diffraction[21–23] and are depicted schematically in Fig. 1: at 0.50 ML a zigzag-like $(4\times2)-4$NO struc-

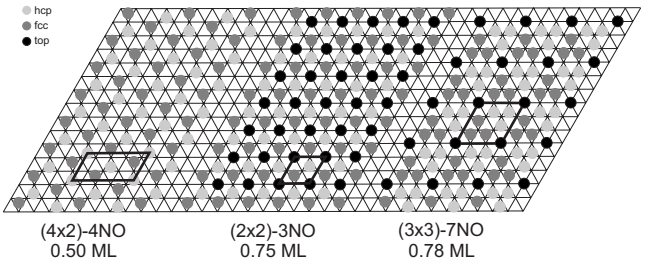

FIG. 1. Top view of experimentally obtained structures of NO on Rh(111) reported in literature. The grid represents the Rh(111) surface: the intersections of the lines symbolize the top Rh atoms and triangles pointing upward (downward) are hcp (fcc) sites. As indicated by the legend, the filled circles represent the NO molecules on one of the three aforementioned adsorption sites. The unit cell of each structure is shown by a black parallelogram. Directly under each structure, its name and coverage are given.

ture was deduced. In this structure the NO molecules are adsorbed in the fcc and hcp sites of the surface.[24] At 0.75 ML, a $(2\times2)-3$NO structure is reported in which the NO molecules occupy the fcc, hcp, and top positions. To our knowledge the only STM study performed on the system of NO on Rh(111) thus far, showed that at room temperature, patches of the 0.78 ML $(3\times3)-7$NO structure (see Fig. 1) started to grow from within the $(2\times2)-3$NO structure as soon as the torr pressure range was reached.[25]

II. EXPERIMENTAL AND COMPUTATIONAL DETAILS

The STM used in this work is a commercial LT-STM from Omicron GmbH. The base pressure in the chamber is $p<10^{-10}$ mbar. Molecules can be deposited *in situ* by a tube connected to a variable leak valve that can be screwed in through a hole in the radiation shields down to a minimum distance of 5 mm from the sample. A clean Rh(111) single crystal was mounted on a sample plate and is cleaned by repeated cycles of Ar^+ sputtering at 500 °C (1.5 μA for 90 min) and annealing at 500, 600 and 700 °C, 20 min for each temperature. The sample was then flashed to 1200 °C. The STM tips are electrochemically etched from polycrystalline tungsten wire ($\oslash$0.35 mm), using the standard etching techniques. After etching, the tips were rinsed with water and blown dry with nitrogen. To remove the tungsten oxide (WNO_3) layer that forms in air, the tips are heated by electron beam bombardment up to temperatures >1200 °C, above which the WNO_3 sublimes and a clean tungsten tip will result.

In the kMC simulation, the surface is represented by a lattice in which every point is labeled according to the type of site (hcp, fcc or top) and its occupation. Such a labeled lattice is called a configuration and can be transformed into another one by means of a reaction. The evolution of the system as a function of time can be described by a master equation:[26]

$$\frac{dP_a(t)}{dt} = \sum_{a\neq b} [k_{ba}P_b(t) - k_{ab}P_a(t)]. \tag{2}$$

Here, $P_a(t)$ denotes the probability to find the system in configuration a at time t; k_{ab} is the transition probability per unit time of the reaction (e.g., adsorption or diffusion) that transfers configuration a into b. This transition probability can be interpreted as a microscopic rate constant and can be described by the Arrhenius equation

$$k_{ab} = \nu_{ab}e^{-E_{\mathrm{act}}/k_BT}, \tag{3}$$

where E_{act} stands for the activation energy, ν_{ab} is the preexponential factor of the reaction that transforms a into b, k_B is Boltzmann's constant, and T is the temperature. Since the occupation of adsorption sites in between two surface rhodium atoms (bridge sites) is not observed experimentally, in our simulations the molecules can only adsorb at the hcp, fcc, and top sites. Reactions that can occur in our system are: adsorption:

$$\mathrm{V}_f \rightarrow \mathrm{NO}_f, \tag{4a}$$

$$\mathrm{V}_h \rightarrow \mathrm{NO}_h, \tag{4b}$$

$$\mathrm{V}_t \rightarrow \mathrm{NO}_t, \tag{4c}$$

diffusion:

$$\mathrm{NO}_f + \mathrm{V}_h \leftrightarrows \mathrm{V}_f + \mathrm{NO}_h, \tag{5a}$$

$$\mathrm{NO}_f + \mathrm{V}_t \leftrightarrows \mathrm{V}_f + \mathrm{NO}_t, \tag{5b}$$

$$\mathrm{NO}_h + \mathrm{V}_t \leftrightarrows \mathrm{V}_h + \mathrm{NO}_t \tag{5c}$$

and desorption:

$$\mathrm{NO}_f \rightarrow \mathrm{V}_f, \tag{6a}$$

$$\mathrm{NO}_h \rightarrow \mathrm{V}_h, \tag{6b}$$

$$\mathrm{NO}_t \rightarrow \mathrm{V}_t, \tag{6c}$$

where V_f, V_h, and V_t stand for a vacant and NO_f, NO_h, and NO_t for an occupied position of type fcc, hcp or top, respectively. As opposed to diffusion and desorption, adsorption is not a thermally activated but a random process of gas molecules impinging on the surface and therefore has no activation barrier [Eq. (3)]. If an NO molecule is adsorbed at an energetically unfavorable site, it will either diffuse away or desorb.

The lateral interactions are included in the simulation by changing the activation energy in the rate Eq. (3) according to

$$E_{\mathrm{act}} = E^0_{\mathrm{act}} + \alpha\left(\sum_n a^f_n\phi_n - \sum_n a^i_n\phi_n\right). \tag{7}$$

Here, E^0_{act} is the activation barrier without lateral interactions, α is the Brønsted-Polanyi parameter, ϕ_n the lateral interaction of type n, and $a^{i(f)}_n$ the number of interactions acting on the molecule in the initial (final) state of the reaction. The parameter α is a measure of how much the lateral interactions influence the activation energy, which is the energy of the transition state in a reaction. It can vary between $0\leq\alpha\leq1$. If the transition state is similar to the initial state, they will both experience the same interactions. Hence, the lateral interactions do not affect these kinds of reactions so

that $\alpha=0$. The lateral interactions have a maximal effect, $\alpha=1$, when the transition state is similar to the final state. In our model, desorption of NO molecules from the Rh(111) surface is direct: molecules go directly to the gas phase and hence, α is taken to be 1. For the process of hopping over the surface from one site to another, α is taken to be 0.5.

The master Eq. (2) is solved using the so-called first reaction method (FRM).[27] In the FRM a list containing all possible reactions is created. The time for each reaction is computed according to

$$\Delta t_{ab} = -\frac{1}{k_{ab}} \ln r, \tag{8}$$

where r is a random number between 0 and 1. Then the following steps are repeatedly carried out:

(1) The reaction with the shortest reaction time is selected from the list of all reactions.

(2) The configuration is adjusted according to the reaction.

(3) The time is set to $t \rightarrow t+\Delta t_{ab}$.

(4) The event list is recomputed.

In principle, the time obtained from Eq. (8) in the kMC simulation can be directly compared to the time of the experiment. However, this can only be done if the reaction constants appearing in Eq. (3) are well known for each reaction. Although some value for the diffusion barrier of NO on Rh(111) has been estimated,[28] due to the exponential behavior of Eq. (3), small deviations from the experimental diffusion barrier will result in orders of magnitude differences in the rate constant. Moreover, the pressure of the NO gas during deposition and hence the adsorption rate cannot be accurately determined in our experiment. Consequently, a direct comparison of times between experiment and simulation can only be done approximately.

However, absolute numbers for the reaction constants are not important for the type of structure that forms. Instead, the formation of a certain structure is completely governed by the difference in free energies between the structures, e.g., the ratio between structures A and B with free energies A_A and A_B on the surface would be $\frac{\theta_A}{\theta_B}=e^{-(A_A-A_B)/k_bT}$. As these energies only depend on temperature and the kinetic parameters, a structural comparison with the experiment can still be made without knowing the exact reaction constants.

The order of magnitude of the prefactors for diffusion and desorption [Eq. (3)] relates to the vibrational frequency of the molecule on the surface and is typically $\sim 10^{13}$ s^{-1}. The activation energy for desorption is chosen to be equal to the adsorption energy of the molecule's adsorption site. Note that at 200 K, with an energy barrier this high, hardly any desorption takes place. The energy barrier of diffusion is chosen such that diffusion is fast enough to form a structure with minimal free energy, but slow enough to speed up the simulation time. The different adsorption energies for the fcc, hcp, and top sites are included in diffusion by changing its barrier accordingly.

III. EXPERIMENTAL RESULTS

At low NO dosage, the surface is partly covered by patches of the $(4\times2)-4$NO structure as is shown in Fig. 2.

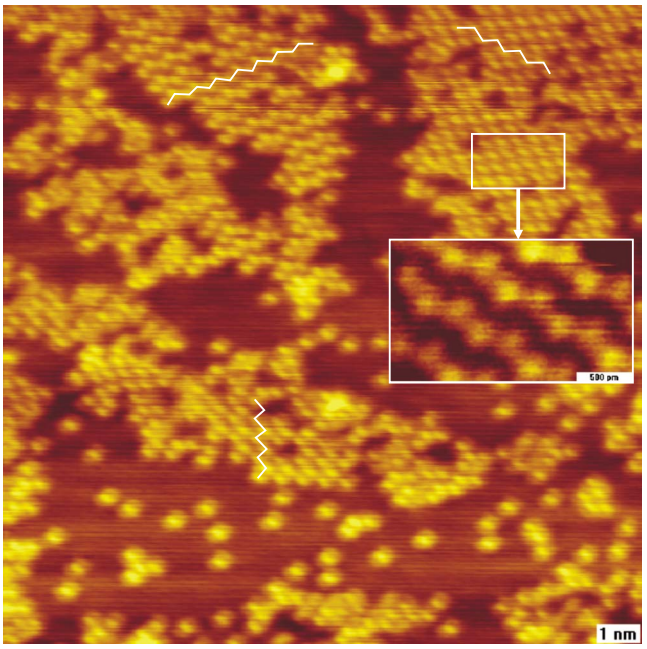

FIG. 2. (Color online) STM image (15×15 nm^2) taken at 77 K of the low coverage phase of NO on Rh(111) deposited at 200 K. About 50% of the surface is covered by single molecules. The other half is ordered in the $(4\times2)-4$NO structure. White zigzag lines are drawn to guide the eye. Inset: 2×1.5 nm^2 zoom on the $(4\times2)-4$NO structure showing individual molecules ($V=109$ mV, $I=416$ pA).

On the Rh(111) surface, there are three possible orientations of the $(4\times2)-4$NO domains, all of which are present in the image as elucidated by the white zigzag lines. The inset is a zoom on a patch in which the individual molecules are resolved. In between the patches, single molecules are found. This structure is in accordance with the reported structure at 0.50 ML.[21–23]

Upon higher dose, the structure of Fig. 3(a) is obtained. The image is a 50×50 nm^2 overview showing lines running all over the sample surface in three different directions. Figure 3(b) is a 15×15 nm^2 zoom on picture (a) emphasizing the linear structure. Three to seven lines run in parallel to each other and in between these lines, features can be discerned that are not imaged as bright as the lines. In zoom shown in the inset, the individual molecules are resolved and white circles are drawn to highlight their position. The structure consists of bright zigzagging lines alternated by straight lines in which the molecules are imaged less bright. This adlayer is therefore identified as a $(\sqrt{3}\times\sqrt{7})-3$NO structure. This previously unreported structure with a coverage of 0.60 ML is shown schematically in Fig. 4. Whereas the adsorption site of the molecules along the zigzag line of the $(4\times2)-4$NO structure alternates between fcc and hcp, here, the zigzag patterns are made up of hcp adsorbed molecules only. In between these wiggly lines, straight lines of wider spaced fcc molecules are formed. The transition from the $(4\times2)-4$NO structure to the $(\sqrt{3}\times\sqrt{7})-3$NO structure is rather fast since it can start from within the $(4\times2)-4$NO domains themselves; i.e., the molecules only have to move closer together without having to reassemble completely.

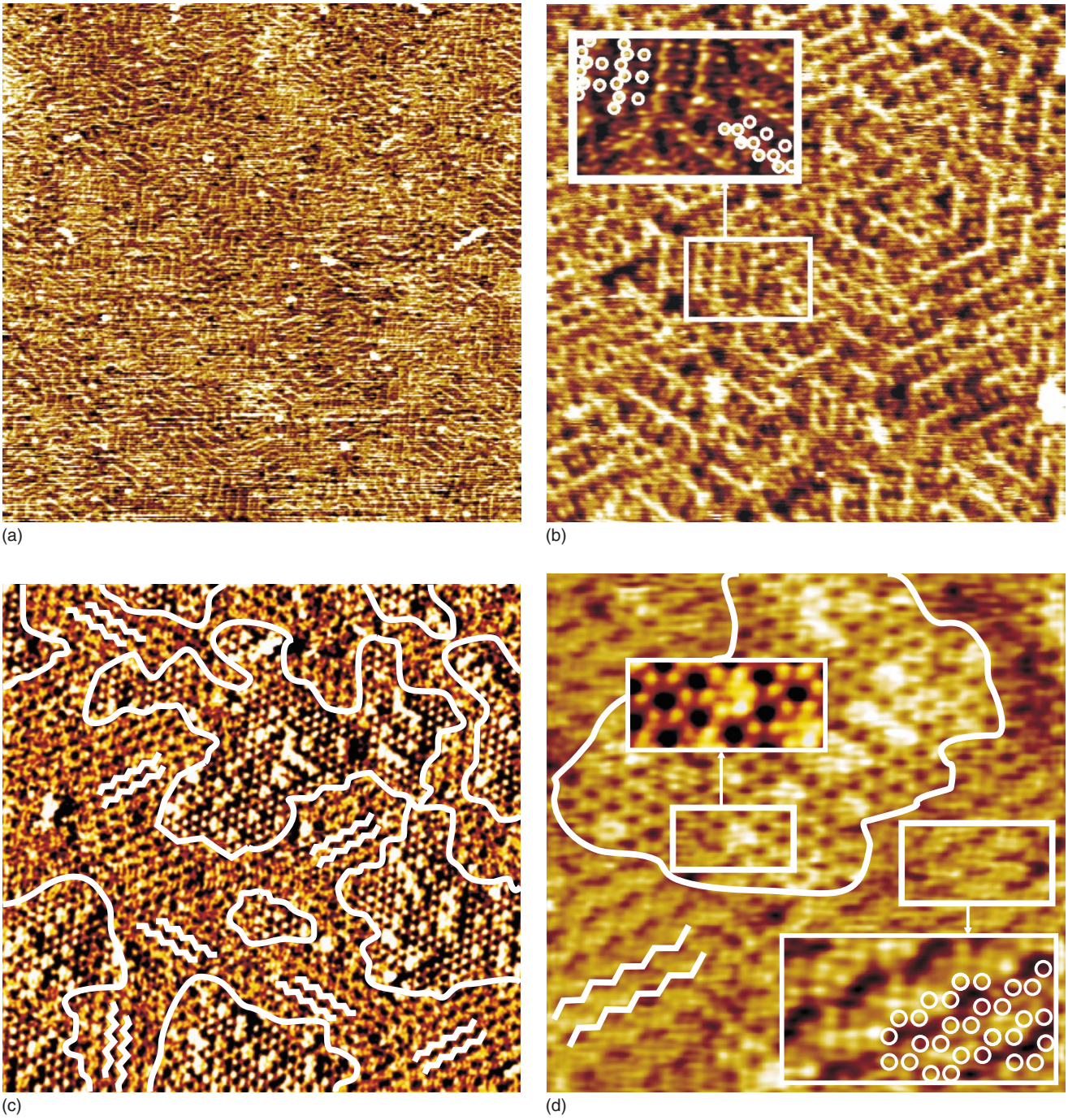

FIG. 3. (Color online) (a) 50×50 nm^2 STM image taken at 200 K showing the linear nature of the adlayer. (b) 15×15 nm^2 zoom on the structure of (a), inset: 6×4 nm^2 zoom resolving the individual molecules of the $(\sqrt{3}\times\sqrt{7})-3$NO structure the positions of which are indicated by the white circles. (c) 30×30 nm^2 image showing two types of structures on the surface. White full lines help to see the boundaries between the different configurations. The wiggly white lines indicate the orientation of the different patches of the zigzag-like structure. (d) 15×15 nm^2 zoom on (c). Left inset: 2.8×1 nm^2 zoom on the $(2\times2)-2$NO structure showing individual molecules. The middle honeycomb is filled by an NO molecule adsorbed on the top site. Lower right inset (4×2 nm^2): Although the individual molecules of the zigzag structure are not well resolved, the positions of the molecules of the $(\sqrt{3}\times3)-4$NO structure, to which this configuration is tentatively assigned, are superimposed as white circles. Measurement parameters for all images: $V=-99$ mV, $I=440$ pA.

In Fig. 3(c), the resulting image is depicted after an even higher dosage of NO to the Rh(111). It shows two different adlayer configurations, separated from each other by white lines to guide the eye. One of the structures again shows a zigzag-like pattern. The different orientations of this structure are indicated by the white zigzag lines. The other structure has a hexagonal symmetry and about one fifth of the pattern is covered by bright dots. Figure 3(d) is a zoom on Fig. 3(c). The inset in the lower right corner is a zoom on the zigzag structure. Although it is hard to identify the individual

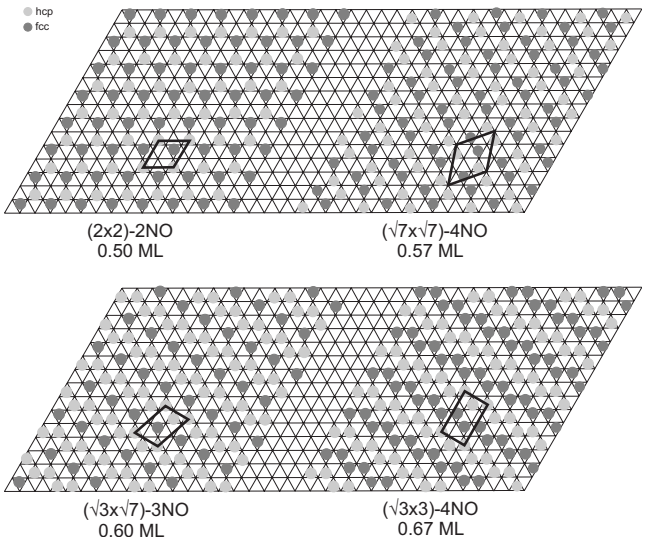

FIG. 4. Top view of ordered structures of NO on Rh(111) obtained in this study. The representation of the structures is similar to Fig. 1.

molecules in the image, this structure is tentatively assigned to the $(\sqrt{3}\times 3)-4$NO structure. The schematic diagram of this unreported $(\sqrt{3}\times 3)-4$NO structure with a coverage of 0.67 ML is also depicted in Fig. 4. A projection of the positions of the molecules of the $(\sqrt{3}\times 3)-4$NO structure in the lower right inset of Fig. 3(d) gives a reasonable match. Similar to the transition from the $(4\times 2)-4$NO structure to the $(\sqrt{3}\times\sqrt{7})-3$NO structure, the transformation from the $(\sqrt{3}\times\sqrt{7})-3$NO to the $(\sqrt{3}\times 3)-4$NO structure can happen within the $(\sqrt{3}\times\sqrt{7})-3$NO patch itself: the lines only need to move closer together. The hexagonal structure could be resolved with molecular resolution as is shown in the left inset of Fig. 3(d). The molecules are arranged in a honeycomb structure, similar to the $(2\times 2)-2$NO structure of Fig. 4. The blurry bright spots in the patch arise from top bound NO molecules at the center of the honeycombs. This means that the structure is actually a mixture between the 0.50 ML $(2\times 2)-2$NO and 0.75 ML $(2\times 2)-3$NO configurations (compare Figs. 1 and 4).

Figure 5 shows the diffusion at 200 K of the top bound NO molecules in the $(2\times 2)-2$NO structure over time. Isolated top molecules make multiple hops from one honeycomb to another within minutes. Apparently, the physical barrier formed by the two NO molecules at the fcc and hcp sites does not prevent the molecule from diffusing. From this figure, we can estimate the activation barrier for this type of diffusion by rewriting Eq. (3):

$$E_{\mathrm{act}} = -k_b T \ln\frac{k_{\mathrm{diff}}}{\nu}. \tag{9}$$

From Fig. 5, the rate constant for top diffusion of an isolated top bound NO molecule can be estimated to be of the order of $k_{\mathrm{diff}}\sim 0.01\ \mathrm{s}^{-1}$. A typical value for the prefactor ν is $\sim 10^{13}\ \mathrm{s}^{-1}$ and with $T=200$ K this amounts to $E_{\mathrm{act}}=70$ kJ/mol. The error of this calculation depends on the uncertainty of the determination of k_{diff} and ν. However, as

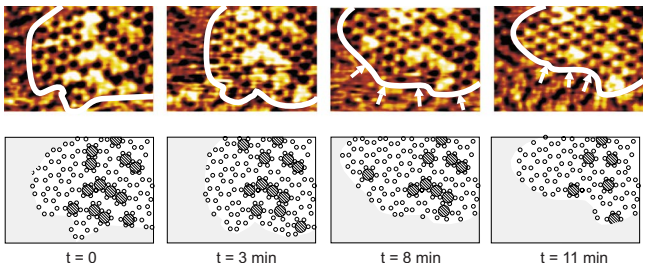

FIG. 5. (Color online) Sequence of 4×3 nm^2 STM images taken at 200 K ($V=99$ mV, $I=440$ pA) to illustrate the diffusion of the top adsorbed NO molecules over the $(2\times 2)-2$NO structure. The white lines mark the boundary between the $(2\times 2)-2$NO and $(\sqrt{3}\times 3)-4$NO configurations. The movement of this boundary over time is indicated by the white arrows. For clarity, the bottom row is a schematic representation of the STM images. The open circles stand for the NO molecules in the $(2\times 2)-2$NO structure. The larger dashed circles depict the top bound molecules and the gray area is the area of the $(\sqrt{3}\times 3)-4$NO structure.

E_{act} depends only logarithmically on the ratio $\frac{k_{\mathrm{diff}}}{\nu}$, even if our estimate is off by 2 orders of magnitude, the error in the activation barrier is still only 13%.

It is remarkable that the dilute 0.50 ML $(2\times 2)-2$NO structure forms at high exposures of the substrate to the NO gas. After all, as was shown in Fig. 2, at 0.50 ML coverage, it is the $(4\times 2)-4$NO structure that prevails. Taking into account the higher density of the coexisting $(\sqrt{3}\times 3)-4$NO structure, the appearance of the $(2\times 2)-2$NO patches cannot be explained as a transition structure in the transformation from the $(\sqrt{3}\times 3)-4$NO structure to the denser 0.75 ML $(2\times 2)-3$NO adlayer. Even when accounting for the fact that about one fifth of the honeycombs in Fig. 3(d) is filled, this still amounts to a coverage of only 0.55 ML. Taking a closer look at Fig. 5, however, the patch of the $(2\times 2)-2$NO structure is decreasing in size over time, as is illustrated by the arrows in the consecutive images. This means that the system is undergoing a phase transition. Probably, the exposure of the substrate to a relatively high NO gas pressure resulted in patches of the 0.67 ML $(\sqrt{3}\times 3)-4$NO and the 0.75 ML $(2\times 2)-3$NO structures. However, when the NO gas was removed from the chamber prior to starting the experiment, the system had to reach a different equilibrium. The molecules adsorbed at the top sites of the $(2\times 2)-3$NO structure have the weakest bond to the substrate and will therefore desorb first, leaving the patch behind in the $(2\times 2)-2$NO configuration. Being instable, this configuration slowly transforms into the $(\sqrt{3}\times 3)-4$NO structure, as is observed in Fig. 5.

IV. SIMULATION AND DISCUSSION

Parallel to the experimental work, the kinetic parameters (i.e., lateral interactions and adsorption energies) of NO on Rh(111) used in our kMC simulations have been determined from 74 adlayer structures with different coverages.[29] The total number of kinetic parameters (i.e., the adsorption energies and the pairwise, three and four particle interactions) to

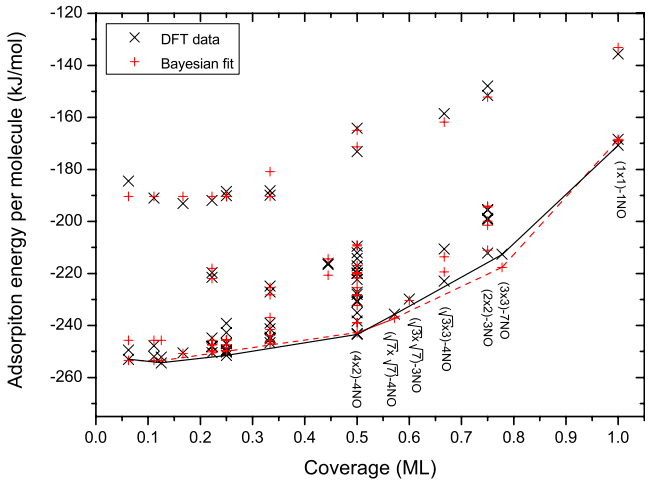

FIG. 6. (Color online) Graph showing the zero temperature phase diagram (Ref. 29). Each of the 73 (black) cross symbols represents the DFT calculated adsorption energy per molecule for a structure of a certain coverage. The (red) plus symbols denote the adsorption energy calculated from the fitted kinetic parameters. The full and dashed lines connect data points of the structures with minimum energy for the DFT calculated and fitted values, respectively.

take into account in the kMC simulations is 13. Furthermore, only the short range pair interactions with the next-nearest and next-next-nearest neighbors seem to be important. As the hcp site has the lowest binding energy, this site becomes occupied first at low coverage. It is therefore reasonable also to expect the longer range pair interactions to exist for the hcp site only. Finally, next to the pair interactions, homogeneous linear three particle interactions for the hcp and fcc sites appear to be important, but all other three and four particle interactions do not play a role.

A. Zero-temperature phase diagram

In Ref. 29 the phase diagram of NO on Rh(111) at $T=0$ K as a function of coverage is derived; see Fig. 6. Each (black) cross symbol in the graph represents the DFT calculated adsorption energy per NO molecule of a structure. The (red) plus symbols indicate the adsorption energy calculated using the fitted kinetic parameters. The (black) full line connects the DFT calculated data points that have the lowest energy of adsorption with the lowest possible slope. The (red) dashed line similarly connects the fitted data points. Although somewhat deviating in energy, the points connected by both lines represent the same structures. In the coverage range 0.50–0.80 ML, each point with the lowest adsorption energy is labeled according to the name of the structure it belongs to. The configuration for each of these structures is shown in Figs. 1 and 4.

The zero-temperature phase diagram of Fig. 6 shows what structure is energetically most favorable. For example, at 0.50 ML coverage, this will be the $(4\times2)-4$NO structure and at 0.78 ML the $(3\times3)-7$NO configuration. An adlayer with a coverage on the line drawn between two data points will consist of patches of the two structures belonging to these data points. The area occupied by each patch is inversely proportional to the distance to the data point to which the structure corresponds.

As is explained by Eq. (1), at finite temperatures, the phase diagram might start to deviate from Fig. 6. In order to include the entropy, kMC simulations were performed. The nearest-neighbor interaction with NO's at different types of sites could not be determined because, in the DFT calculation, structures with NO molecules located this close together were unstable.[29] Therefore, for this interaction, a value close to the desorption energy of a hollow site is chosen. This ensures desorption of a molecule when it is experiencing a nearest-neighbor interaction but is impeded to diffuse away due to other neighboring molecules.

Note that when structures in kMC were found that had not been included in the DFT derivation of the lateral interactions, the interactions had to be determined again including the omitted structure. This procedure was repeated until all configurations found in kMC have been used for deriving the lateral interactions.[30]

B. Kinetic Monte Carlo simulations

The resulting structures of the kMC simulation performed at 200 K are shown in Figs. 7–10 for increasing coverage of the surface. Increasing the coverage is achieved by increasing the adsorption rate of the molecules on the surface. The diffusion rate constant was always chosen such that the layer stayed in equilibrium during the simulation.

Just as in Fig. 1, the brightest dots in the images denote the hcp bound molecules, the dark gray dots the fcc molecules, and the black dots the top bound molecules. At an overall coverage of around 0.40 ML, the first ordered patches start to form. In Fig. 7, it is shown that these patches consist of the 0.50 ML $(4\times2)-4$NO structure. The zigzag lines in the picture help to see the orientation of the different domains. Indeed, based on the zero-temperature phase diagram of Fig. 6, this structure would have been expected to form at 0.50 ML coverage. Comparing Fig. 2 to the simulated adlayer of Fig. 7, both images show patches of the $(4\times2)-4$NO structure of different orientation. Moreover, this structure has been repeatedly reported in literature.[21–23] In the kMC image the formation of $(4\times2)-4$NO patches started at a total coverage of about 0.40 ML. This can be understood by realizing that all lateral interactions are repulsive.[29] Therefore, the molecules would like to stay as far apart as possible. Only when approaching 0.50 ML coverage, the optimal solution is the formation of the $(4\times2)-4$NO structure. In the experimental image of Fig. 2 the coverage is estimated to be 0.30 ML but islands of the $(4\times2)-4$NO structure are already formed despite the fact that there is still space for the molecules to spread out further in between the patches. This difference might be explained by the presence of subsurface impurities that are known to serve as nucleation centers for CO on Pd(111).[31] The subsurface density of our sample is estimated to be less then 2%, so that the 15×15 nm^2 image in Fig. 2 is expected to have less than 50 nucleation sites, in accordance to the observation. Yet, the fact that these impurities cause premature nucleation of domains does not seem to affect the type of structure that is formed.

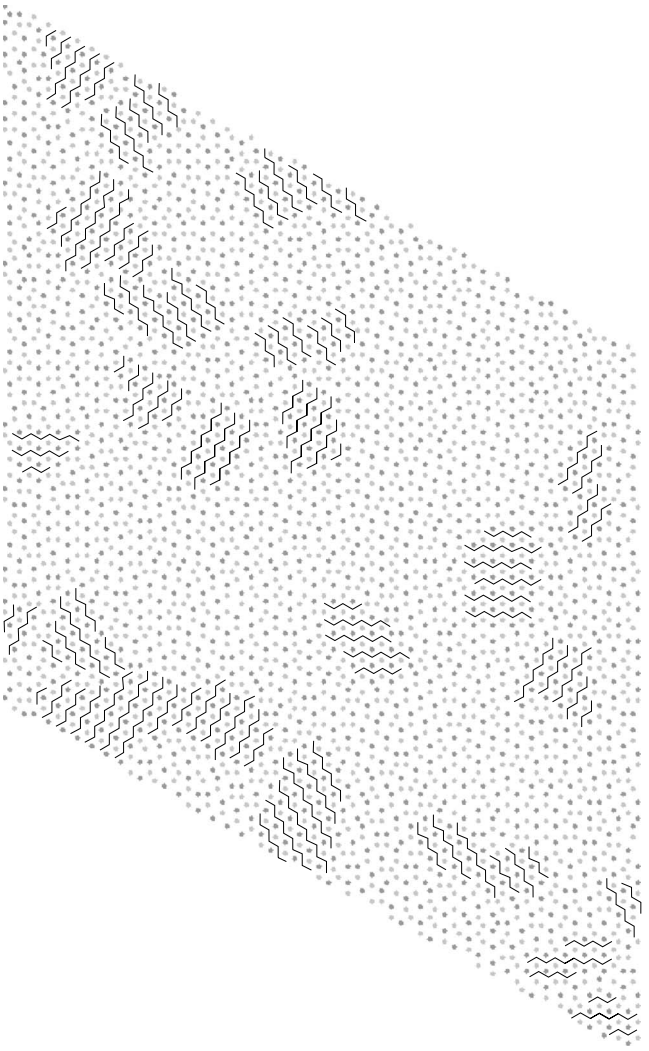

FIG. 7. Adsorbate distribution from the kMC simulation at $T=200$ K and $\theta=0.54$ ML showing patches of the $(4\times2)-4$NO structure of different orientation. The zigzag lines are drawn to guide the eye. Each side of the parallelogram is 20.5 nm.

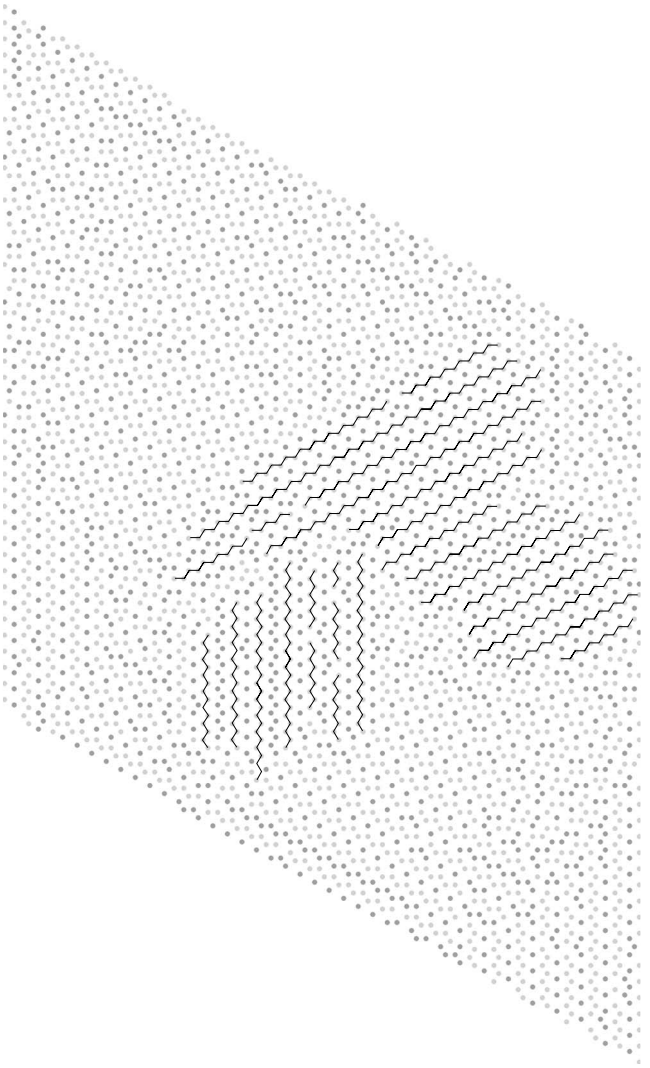

FIG. 8. Adsorbate distribution from the kMC simulation at $T=200$ K and $\theta=0.61$ ML. The dominant structure is the $(\sqrt{3}\times\sqrt{7})-3$NO with small areas of the $(\sqrt{3}\times3)-4$NO structure. The zigzag lines are drawn to guide the eye. Each side of the parallelogram is 20.5 nm.

When increasing the coverage, the $(4\times2)-4$NO structure transforms into another zigzag-like structure, as depicted in Fig. 8. To guide the eye, the hcp zigzag lines are highlighted in parts of the adlayer of Fig. 8. The resemblance between this $(\sqrt{3}\times\sqrt{7})-3$NO configuration and Fig. 3(b) is striking. According to Fig. 6, at $T=0$ K, the $(\sqrt{7}\times\sqrt{7})-4$NO structure would be preferred to form above the $(\sqrt{3}\times\sqrt{7})-3$NO structure, which is located slightly above the minimum energy line. This discrepancy can be explained by the entropy of the $(\sqrt{3}\times\sqrt{7})-3$NO being larger than the entropy of the $(\sqrt{7}\times\sqrt{7})-4$NO adlayer, as was explained in Eq. (1).

Figure 9 shows that a further increase in coverage amounts to the formation of the $(\sqrt{3}\times3)-4$NO structure (see Fig. 4). During the transition between the $(\sqrt{3}\times\sqrt{7})-3$NO and the $(\sqrt{3}\times3)-4$NO structure, the density along the line formed by the fcc molecules is doubled by transforming from a straight line into a zigzag line. In parts of the picture of Fig. 9, the zigzag pattern is indicated by zigzag lines. Comparing Fig. 3(c) to Fig. 9, both pictures show patches in which several zigzag lines run parallel to each other. Similar to the transition from the $(4\times2)-4$NO structure to the $(\sqrt{3}\times\sqrt{7})-3$NO structure, the transformation from the $(\sqrt{3}\times\sqrt{7})-3$NO to the $(\sqrt{3}\times3)-4$NO structure can happen within the $(\sqrt{3}\times\sqrt{7})-3$NO patch itself: the lines only need to move closer together. In fact, in Fig. 8, some areas of the $(\sqrt{3}\times3)-4$NO structure can already be discerned. Just as the $(\sqrt{3}\times\sqrt{7})-3$NO, the $(\sqrt{3}\times3)-4$NO structure is located slightly above the line of minimal energy in Fig. 6 but can be accounted for by the entropy.

Comparing Fig. 9 to Fig. 3(d), there is a close match as far as the 0.67 ML $(\sqrt{3}\times3)-4$NO is concerned. However, a mix of the $(\sqrt{3}\times3)-4$NO with the 0.50 ML $(2\times2)-2$NO structure could not be obtained in the simulations. As discussed in the experimental section, this is an instable structure resulting from the desorption of the top molecules from the 0.75 ML $(2\times2)-3$NO configuration. Based on Fig. 3(d), the $(2\times2)-3$NO structure is expected at higher coverages.

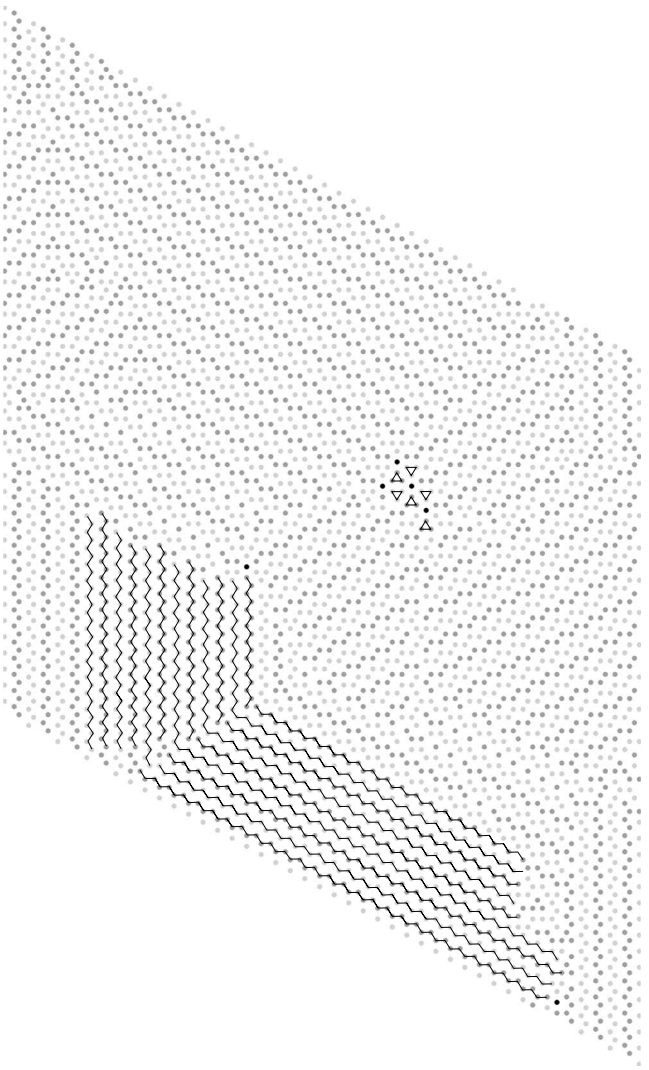

FIG. 9. Adsorbate distribution from the kMC simulation at $T=200$ K and $\theta=0.67$ ML showing the $(\sqrt{3}\times 3)-4$NO structure. The zigzag lines guide the eye. Each side of the parallelogram is 20.5 nm. In the middle of the picture, at the boundary between two grains, a seed of the $(3\times 3)-7$NO is already visible as indicated by the triangles.

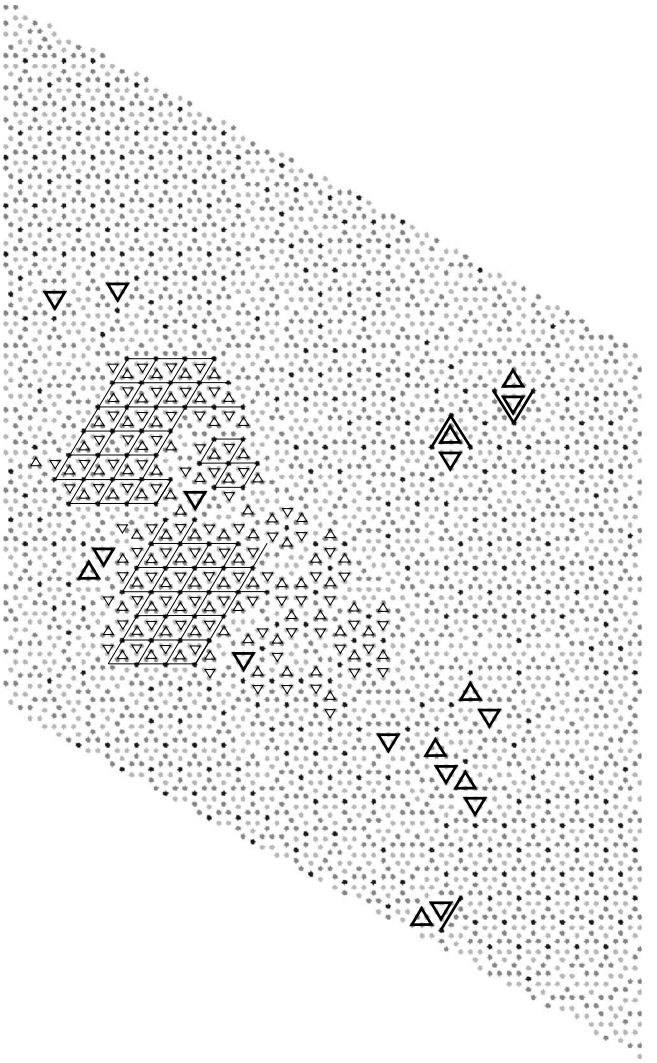

FIG. 10. Adsorbate distribution from the kMC simulation at $T=200$ K and $\theta=0.76$ ML showing patches of the $(3\times 3)-7$NO structure. The configuration is indicated by the lines connecting the top molecules and triangles highlighting the groups of fcc and hcp molecules. The large triangles highlight groups consisting of six fcc and hcp molecules. Each side of the parallelogram is 20.5 nm.

However, the obtained structure is the 0.78 ML $(3\times 3)-7$NO as depicted in Fig. 10. In some areas of the figure, the $(3\times 3)-7$NO structure is indicated by lines connecting the top molecules and triangles illustrating the triangular arrangement of the fcc and hcp molecules.

Although this structure was reported experimentally at room temperature in the torr pressure range,[25] the $(2\times 2)-3$NO structure has been reported in many other experimental studies next to this work.[21–23,25,32] Several reasons for this mismatch between theory and experiment can be given. First, it can be attributed to the error in the DFT calculations. According to the Bayesian analysis,[29] the average error of all the DFT calculated adlayer configurations is 3.5 kJ/mol, which is comparable to the difference in adsorption energy between the $(2\times 2)-3$NO and $(3\times 3)-7$NO structure; see Fig. 6. Being an average value, the error for these specific structures could be even larger, resulting in the preference for the $(3\times 3)-7$NO structure. Alternatively, it is known that DFT calculations underestimate the stability of CO molecules bound to top adsorption sites.[33] If this is also true for NO molecules, the adsorption energy for the $(2\times 2)-3$NO structure would be calculated to be higher than the adsorption energy of the $(3\times 3)-7$NO configuration since it has more top adsorbed molecules per unit area. Finally, deviations between the DFT calculated adsorption energies and the adsorption energies calculated from the fitted kinetic parameters might be the cause; see Fig. 6. Overall, the fitted data points match the DFT values rather well. However, the fitted adsorption energy for the $(3\times 3)-7$NO configuration is well below the DFT calculated point. As a result, this is the point where both lines of minimal adsorption energy deviate most. Consequently, the difference in adsorption energy at 0.75 ML between the data point of the $(2\times 2)-3$NO structure and the (red) dashed line is approximately two times

TABLE I. The time it takes to form the structures of Figs. 7–10. The times are scaled to $k_{ads}=1\ s^{-1}$ to make them comparable. The times are inversely proportional to k_{ads}. The transition factor in the last column is the ratio of the time of formation between the structure before and after the transition.

Structure	Scaled kMC time	Transition factor
$(4\times2)-4NO$	2.5 s	
		⇕15×
$(\sqrt{3}\times\sqrt{7})-3NO$	37.5 s	
		⇕13×
$(\sqrt{3}\times3)-4NO$	8.3 min	
		⇕195×
$(3\times3)-7NO$	27 h	

larger than for the (black) full line. This energy difference could be too large for the entropy to overcome and hence, the $(3\times3)-7NO$ structure is favored to form.

As opposed to the previously discussed transitions, the transition from the $(\sqrt{3}\times3)-4NO$ to the $(3\times3)-7NO$ structure is slow as the molecules have to rearrange completely. Therefore this structure can only start growing from the boundaries between the different patches of the $(\sqrt{3}\times3)-4NO$ structure. In some parts of Fig. 10 some small grains of a 0.81 ML $(4\times4)-13NO$ structure can be seen. This structure has a similar molecular arrangement as the $(3\times3)-7NO$ structure. The top atom sits at the corner of the unit cell with two triangular groups of six molecules adsorbed at the fcc and hcp sites each. In the picture of Fig. 10, the $(4\times4)-13NO$ structure is indicated by thick lines in a similar way as for the $(3\times3)-7NO$ configuration.

In Table I it is shown how much time it takes for a certain structure to form in the kMC simulations of Figs. 7–10. In order to make a proper comparison, all simulation times are scaled to an adsorption rate of $k_{ads}=1\ s^{-1}$. In the last column, the transition factor indicates how much time it takes for a structure to form during a phase transition between two structures. It is expressed in multiples of the formation time of the phase before the phase transition took place. Indeed, the transitions described before as being fast have a transition factor of about 15 whereas for the slow transition from the $(\sqrt{3}\times3)-4NO$ to the $(3\times3)-7NO$ structure it is 195.

It is interesting to note that in Ref. 34 the saturation coverage of NO on Rh(111) at $T=120$ K and $p=10^{-7}$ mbar was determined to be 0.68 ML. The configuration of this adlayer, however, could not be derived. At 120 K, diffusion is slow and it might therefore be expected that only the easy transformations can occur within a reasonable amount of time. The configuration with the highest possible structure that can be obtained this way is the $(\sqrt{3}\times3)-4NO$ structure with a coverage of 0.67 ML, in accordance to the experimentally determined value.

Our kMC simulations can be compared directly to a similar theoretical study on the same system, in which only pairwise interactions up to the next-next-nearest neighbor were taken into account.[10] There, at 0.50 ML coverage, the formation of either the $(4\times2)-4NO$ or the $(2\times2)-2NO$ structure, which is depicted in Fig. 4, strongly depended on the value of the next-next-nearest neighbor. Due to the error margin of the calculation this value could not be determined. The $(2\times2)-2NO$ structure on average has 1.5 next-next-nearest neighbors per adsorbate, whereas the $(4\times2)-4NO$ structure has only 1. Large repulsive interactions of 5 kJ/mol therefore resulted in the $(4\times2)-4NO$ structure. For interactions of the order of the simulation temperature of 200 K (2 kJ/mol), however, islands of both structures were observed. A structure with high density was then easily formed by filling the honeycombs of the $(2\times2)-2NO$ structure with top bound NO molecules, resulting in the 0.75 ML $(2\times2)-3NO$ structure (Fig. 1). However, in Ref. 29 it is revealed that the next-next-nearest neighbor interaction is 4 kJ/mol, too large for the $(2\times2)-2NO$ structure to be formed at 0.50 ML as is shown in Fig. 7.

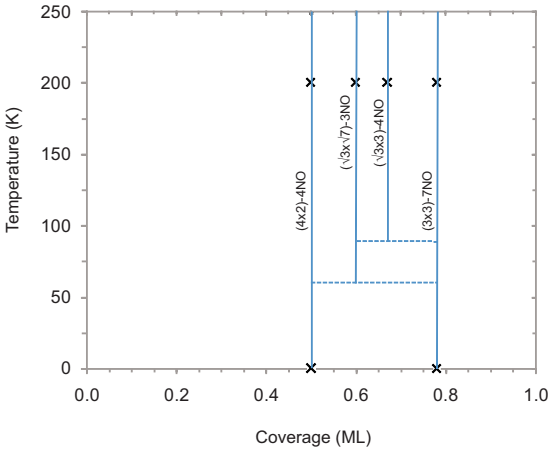

FIG. 11. (Color online) Graph showing a rough sketch of the finite temperature phase diagram. The black crosses represent phase transitions based on information in this paper at $T=0$ K and $T=200$ K. The vertical lines are drawn to extrapolate the diagram to other temperatures. Dashed horizontal lines are drawn at an arbitrary temperature between $T=0$ K and $T=200$ K to indicate the onset of phase transitions.

C. Finite temperature phase diagram

Finally, combining all the data of this paper, a rough sketch can be given for the finite temperature phase diagram of NO on Rh(111); see Fig. 11. Each cross in the graph represents a phase transition that has actually been determined. The phase transitions at $T=0$ K can be derived from the zero-temperature phase diagram of Fig. 6 by following the full (black) or dashed (red) line. Three areas can be discerned: between 0 and 0.50 ML the adlayer consists of a mix of disordered molecules and the $(4\times2)-4NO$ structure. Between 0.50 ML and 0.78 ML coverage, there is a mix between the $(4\times2)-4NO$ and $(3\times3)-7NO$ structures. Lastly, between 0.78 ML and 1.0 ML, it is a mix of the $(3\times3)-7NO$ and the $(1\times1)-1NO$.

At $T=200$ K, the phase transitions are derived from the kMC simulations. Next to the $(4\times2)-4NO$ and $(3\times3)-7NO$ structures, the $(\sqrt{3}\times\sqrt{7})-3NO$ and $(\sqrt{3}\times3)-4NO$ structures have emerged, giving rise to four phase transitions

at $T=200$ K: two of them are similar to the zero-temperature phase transitions and can therefore be connected by a vertical line. The text at the vertical line denotes the structure the rhodium would be fully covered with. The two transitions make up two boundaries between the $(4\times2)-4$NO and $(3\times3)-7$NO structures: one indicating an area with a mixture of the $(4\times2)-4$NO and $(\sqrt{3}\times\sqrt{7})-3$NO structure and the other one an area with a mixture of the $(\sqrt{3}\times\sqrt{7})-3$NO and the $(\sqrt{3}\times3)-4$NO structures.

It is unknown at what temperatures the two phase transitions start to emerge. Therefore the onset is indicated by a dashed horizontal line at an arbitrary temperature between $T=0$ K and $T=200$ K. In Fig. 11, it is indicated that the $(\sqrt{3}\times\sqrt{7})-3$NO structure starts to show up at lower temperatures than the $(\sqrt{3}\times3)-4$NO, but it could well be the other way around.

V. CONCLUSION

In this work, the interaction parameters of NO molecules adsorbed on a Rh(111) substrate are obtained from DFT calculated structures. It is shown that pairwise and homogeneous three particle interactions are important and that heterogeneous three and homogeneous four particle interactions do not play a role. Deviations from the zero-temperature phase diagram as a result of entropy effects are studied by kinetic Monte Carlos simulations. Experimentally, structures with different coverage are studied by STM and compared to the simulations. The first adlayer structure that is found to form is the well-known 0.50 ML $(4\times2)-4$NO configuration. The onset of patch formation is observed at 0.30 ML in the experiment whereas theoretically domain growth starts at 0.40 ML. This difference is attributed to subsurface impurities in the rhodium single crystal that serve as nucleation centers. In the simulations, two structures were found at coverages of 0.60 ML and 0.67 ML that were confirmed experimentally. As these three structures all have a similar zigzag-like nature, the transition between them can be performed without a complete reordering of the molecules. Yet, these rearrangements are necessary when going to higher coverage. At these densities, however, the kinetic Monte Carlo simulations did not produce the experimentally observed 0.75 ML $(2\times2)-3$NO structure but instead a 0.78 ML $(3\times3)-7$NO configuration formed. In the STM experiment at 200 K, a metastable 0.50 ML $(2\times2)-2$NO structure was observed that seems to have originated from desorption of the top molecules of the $(2\times2)-3$NO structure. The few top molecules that remained were found to diffuse over the honeycombs of the $(2\times2)-2$NO structure on a time scale of minutes.

ACKNOWLEDGMENT

J.H. would like to thank FOM for financial support.

*c.f.j.flipse@tue.nl

[1] T. L. Einstein and J. R. Schrieffer, Phys. Rev. B **7**, 3629 (1973).
[2] H. P. Bonzel, Surf. Sci. Rep. **8**, 43 (1988).
[3] S. J. Lombardo and A. T. Bell, Surf. Sci. Rep. **13**, 3 (1991).
[4] W. A. Brown, R. Kose, and D. A. King, Chem. Rev. **98**, 797 (1998).
[5] R. Brako and D. Sokcevic, Surf. Sci. **454-456**, 623 (2000).
[6] M. L. Merrick, W. Luo, and K. A. Fichthorn, Prog. Surf. Sci. **72**, 117 (2003).
[7] J. K. Nørskov, *Coadsorption, Promotors and Poisons* (Elsevier, Amsterdam, 1993).
[8] R. M. van Hardeveld, R. A. van Santen, and J. W. Niemantsverdriet, J. Phys. Chem. B **101**, 7901 (1997).
[9] J. T. Stuckless, C. E. Wartnaby, N. Al-Sarraf, S. J. Dixon-Warren, M. Kovar, and D. A. King, J. Chem. Phys. **106**, 2012 (1997).
[10] C. G. M. Hermse, F. Frechard, A. P. van Bavel, J. J. Lukkien, J. W. Niemantsverdriet, R. A. van Santen, and A. P. J. Jansen, J. Chem. Phys. **118**, 7081 (2003).
[11] T. T. Tsong, Phys. Rev. Lett. **31**, 1207 (1973).
[12] F. Watanabe and G. Ehrlich, Phys. Rev. Lett. **62**, 1146 (1989).
[13] J. Trost, T. Zambelli, J. Wintterlin, and G. Ertl, Phys. Rev. B **54**, 17850 (1996).
[14] J. Repp, F. Moresco, G. Meyer, K. H. Rieder, P. Hyldgaard, and M. Persson, Phys. Rev. Lett. **85**, 2981 (2000).
[15] N. Knorr, H. Brune, M. Epple, A. Hirstein, M. A. Schneider, and K. Kern, Phys. Rev. B **65**, 115420 (2002).
[16] L. Osterlund, M. O. Pedersen, I. Stensgaard, E. Laegsgaard, and F. Besenbacher, Phys. Rev. Lett. **83**, 4812 (1999).
[17] L. Köhler, G. Kresse, M. Schmid, E. Lundgren, J. Gustafson, A. Mikkelsen, M. Borg, J. Yuhara, J. N. Andersen, M. Marsman, and P. Varga, Phys. Rev. Lett. **93**, 266103 (2004).
[18] T. J. Stasevich, T. L. Einstein, and S. Stolbov, Phys. Rev. B **73**, 115426 (2006).
[19] W. Luo and K. A. Fichthorn, Phys. Rev. B **72**, 115433 (2005).
[20] J. Wintterlin, J. Trost, R. Schuster, A. Eichler, and J. S. McEwen, Phys. Rev. Lett. **96**, 166102 (2006).
[21] C. T. Kao, G. S. Blackman, M. A. van Hove, and G. A. Somorjai, Surf. Sci. **224**, 77 (1989).
[22] D. G. Castner, B. A. Sexton, and G. A. Somorjai, Surf. Sci. **71**, 519 (1978).
[23] I. Zasada, M. A. van Hove, and G. A. Somorjai, Surf. Sci. **418**, L89 (1998).
[24] The (111) surfaces of fcc metals have an *ABCABC*… stacking sequence. As a result, there are two different threefold coordinated hollow adsorption sites. Hollow sites having an atom directly underneath in the second (*B*) layer are called hcp sites whereas for fcc sites this atom is located in the third (*C*) layer. Top adsorption sites are directly on top of the atoms in the first (*A*) layer.
[25] K. B. Rider, K. S. Hwang, M. Salmeron, and G. A. Somorjai, Phys. Rev. Lett. **86**, 4330 (2001).
[26] J. J. Lukkien, J. P. L. Segers, P. A. J. Hilbers, R. J. Gelten, and A. P. J. Jansen, Phys. Rev. E **58**, 2598 (1998).
[27] www.catalysis.nl/~chembond/kMC
[28] M. Mavrikakis, J. Rempel, J. Greeley, L. B. Hansen, and J. K.

Nørskov, J. Chem. Phys. **117**, 6737 (2002).
[29] A. P. J. Jansen and C. Popa, Phys. Rev. B **78**, 085404 (2008).
[30] In fact, this is how the $(\sqrt{7}\times\sqrt{7})-4$NO, the $(\sqrt{3}\times\sqrt{7})-3$NO, and the $(\sqrt{3}\times 3)-4$NO structures were found in Ref. 29.
[31] M. K. Rose, A. Borg, T. Mitsui, D. F. Ogletree, and M. Salmeron, J. Chem. Phys. **115**, 10927 (2001).
[32] G. Witte, J. Chem. Phys. **115**, 2757 (2001).
[33] G. Kresse, A. Gil, and P. Sautet, Phys. Rev. B **68**, 073401 (2003).
[34] T. W. Root, L. D. Schmidt, and G. B. Fisher, Surf. Sci. **134**, 30 (1983).